## Supporting Information

# Sacrificial ZnO nanorods drive N- and O- dual-doped carbon towards trifunctional electrocatalysts for Zn-air batteries and self-powered water splitting devices

Mohamed Elhousseini Hilal,[a,b,c] Hussein A. Younus,[d,e] Somboon Chaemchuen,[a] Sander Dekyvere,[a,b] Xianci Zeng,[f] Daping He,[f] Jihae Park,[g] Taejun Han,[g] and Francis Verpoort [a,b,g,h*]

*a. State Key Laboratory of Advanced Technology for Materials Synthesis and Processing, Wuhan University of Technology, Wuhan 430070, China*

*b. School of Materials Science and Engineering, Wuhan University of Technology, Wuhan 430070, China*

*c. Chemistry and environment department, Faculty of Science and technology, Sultan Moulay Sliman University, Beni Mellal 23000, Morocco*

*d. Department of Chemistry, Faculty of Science, Fayoum University, Fayoum 63514, Egypt*

*e. College of Materials Science and Engineering, Hunan University, Changsha 410082, China.*

*f. Hubei Engineering Research Center of RF-Microwave Technology and Application, Wuhan University of Technology, Wuhan 430070, China*

*g. Ghent University, Global Campus Songdo, 119 Songdomunhwa-Ro, Yeonsu-Gu, Incheon 406-840, South Korea.*

*h. National Research Tomsk Polytechnic University, Tomsk 634050, Russian Federation*

E-mail: F. Verpoort; francis.verpoort@ghent.ac.kr,

**This Supplementary Information file includes:**

Supplementary Figures S1 to S18

Supplementary Table S1 to S5

References

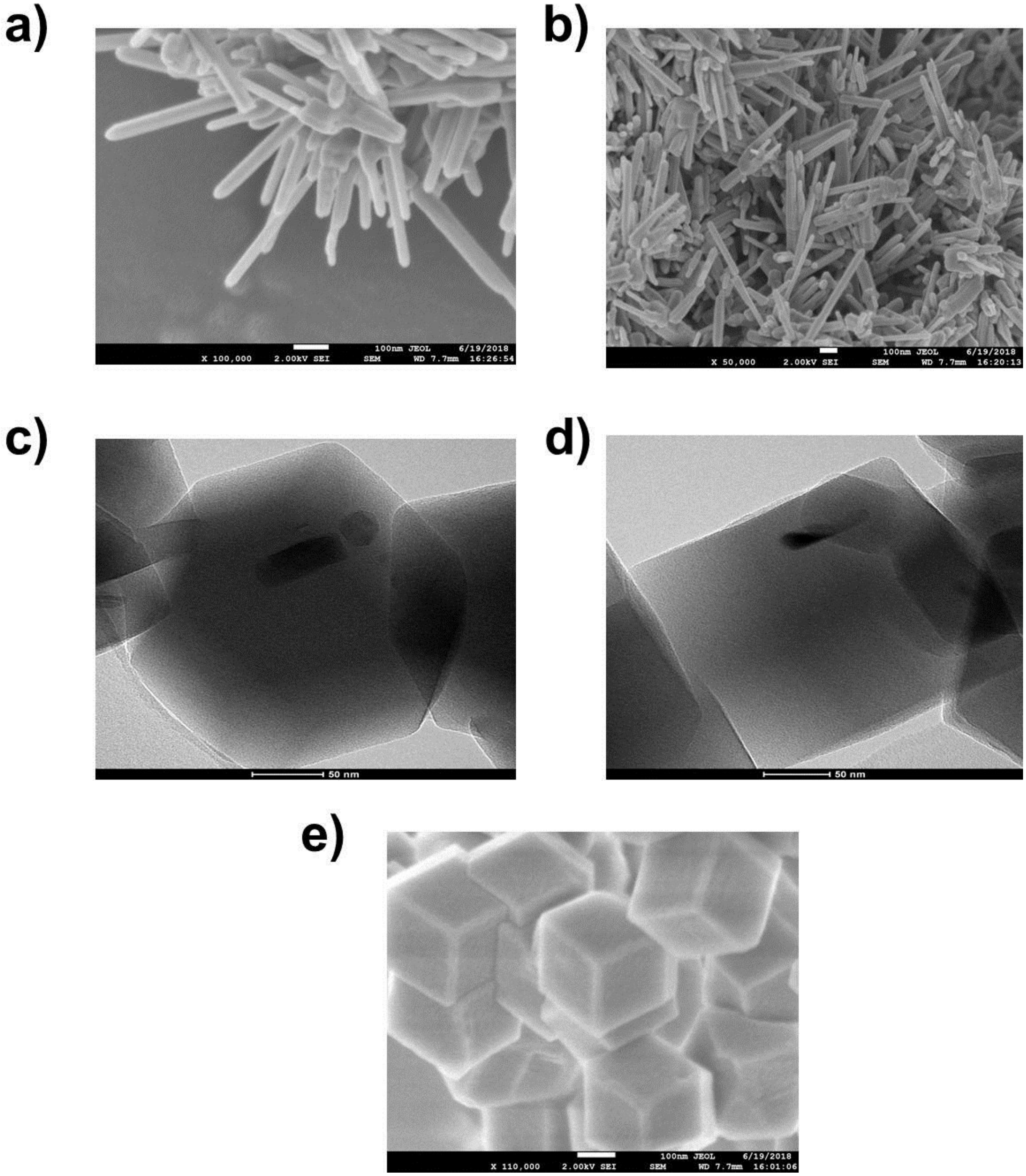


***Figure S1. SEM micrographs of ZnO NRs (a, b); TEM micrographs of ZnONR@ZIF-67 (c, d); and SEM micrographs of ZIF-67 (e).***

It is clear from **Figure** S1a and b that the ZnO nanorods share one base as their growth by thermal decomposition mechanism dictates.[1] Thus, the dispersion of ZnO nanorods in methanol is applied for the purpose of breaking this compact bulky structure to smaller single ZnO nanorods, before the growth of ZIF-67.

This dispersion breaks the nanorods to smaller sizes as visible from inside ZIF-67 polyhedra in **Figure** S1c and d.

It is to note that the nanorods inside ZIF-67 polyhedra cannot have the same size since the breaking happens in a random trend during methanol dispersion. For instance, ZnO nanorods sizes measured in **Figure** S1c and d, are only 69 nm and 71 nm, respectively.

| Average ZnO NR Width (nm) | Average ZnO NR length (nm) |
|---|---|
| 33 (4) | 346 (28) |

| *ZIF-67 Average diameter (nm)* | *ZnONR@ZIF67 Average diameter (nm)* |
|---|---|
| *177 (17)* | *210 (8)* |

***Table S1. The average diameters and lengths of ZnO NR, ZIF-67 and ZnONR@ZIF-67.***

*All the measurements were taken from SEM micrographs and elaborated via ImageJ, the average is displayed on the tables above. ZIF-67 was synthesized with 8:1 mIm/Co nitrates,*[1] *except that it involves no ZnO NR, XRD and SEM characterizations were applied on it for the purpose of comparison.*

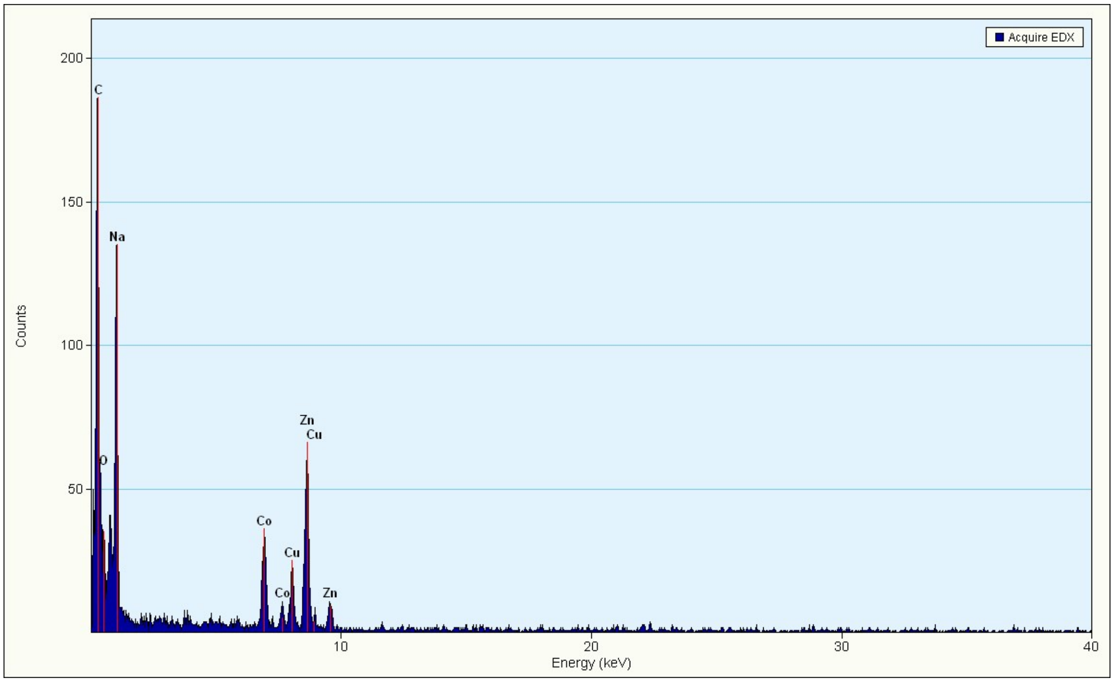


***Figure S2. Localized TEM-EDX spectrum of ZnONR@ZIF-67.*** *The spectrum asserts the presence of zinc, oxygen, cobalt, and carbon, while the presence of Na and Cu is due to the instrument.*

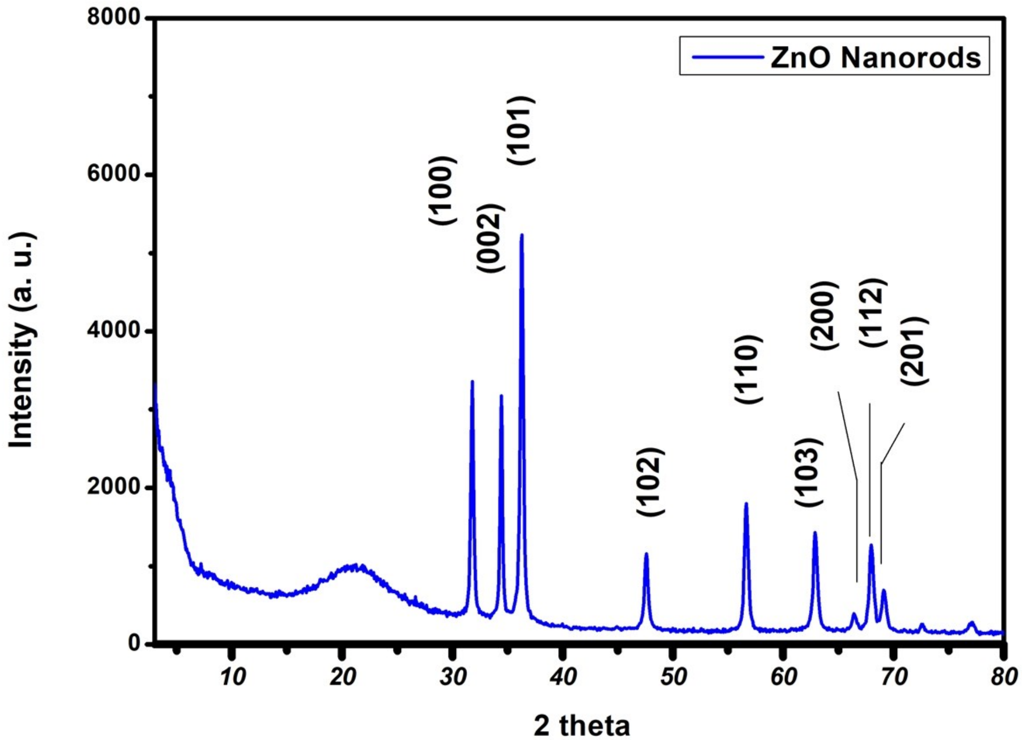


***Figure S3. XRD pattern of synthesized ZnO nanorods.***
This pattern matches ZnO wurtzite phase JCPDS 01-070-8070.

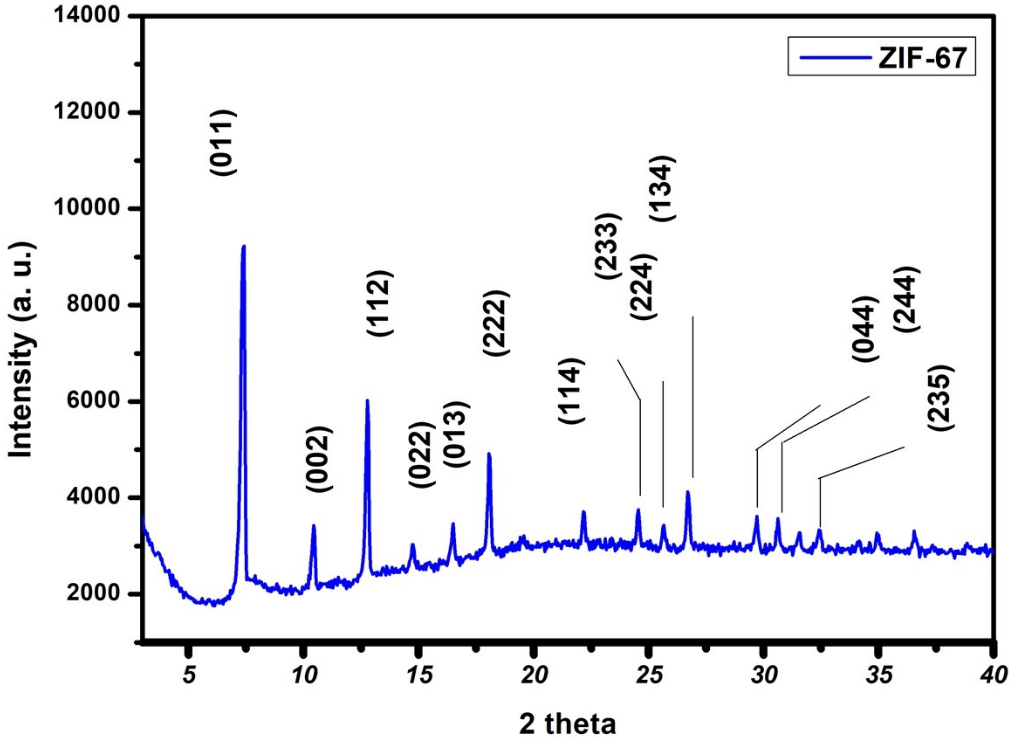


***Figure S4. XRD spectrum of ZIF-67.***

The XRD pattern shows the diffractions of ZIF-67 synthesized with Cobalt metal salt, and 2-mIm with a ratio of 1 to 8, respectively.

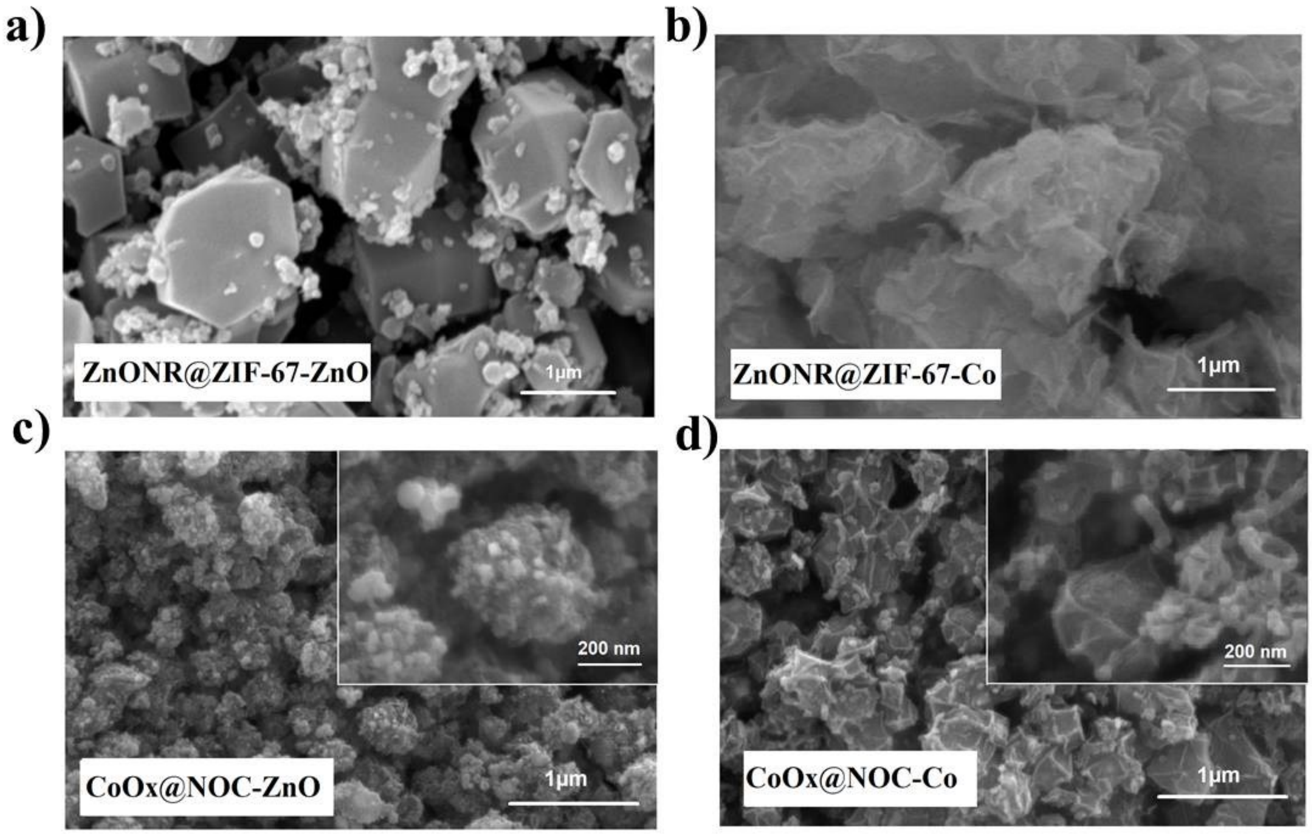


***Figure S5: SEM micrographs of ZnONR@ZIF-67-ZnO (a) and ZnONR@ZIF-67-Co (b) and their adjacent pyrolyzed samples CoOx@NOC-ZnO (c) and CoOx@NOC-Co (d).***

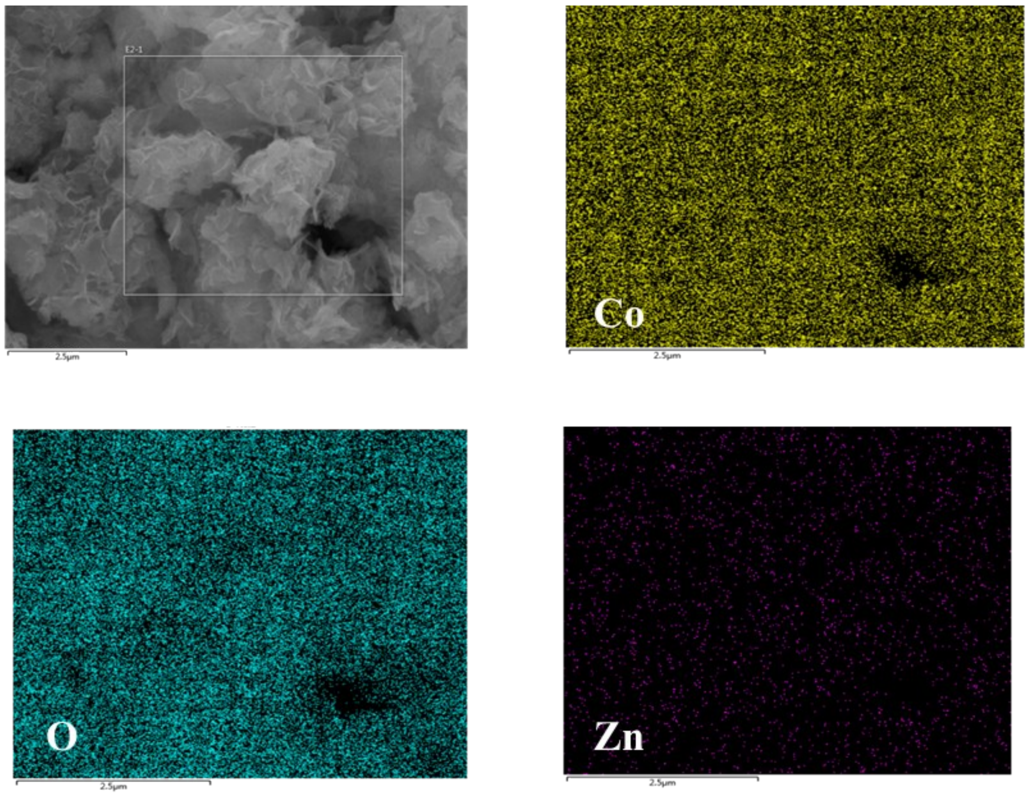


*Figure S6: SEM-EDS mapping of ZnONR@ZIF-67-Co.*

| Elements of the samples | | CoOx@NOC-ZnO | CoOx@NOC | CoOx@NOC-Co | CoOx@NC |
|---|---|---|---|---|---|
| ICP | Zn (%) | 0.12 | 0.051 | 0.032 | - |
| | Co (%) | 20.45 | 24.97 | 31.64 | - |
| Element Analysis | N (%) | 2.63 | 2.32 | 2.08 | 1.2 |
| | C (%) | 47 | 57.69 | 51 | 41 |

***Table S2. The ICP and elemental analysis for the 4 pyrolysed samples, CoOx@NOC-ZnO, CoOx@NOC, CoOx@NOC-Co and Co@NC.***

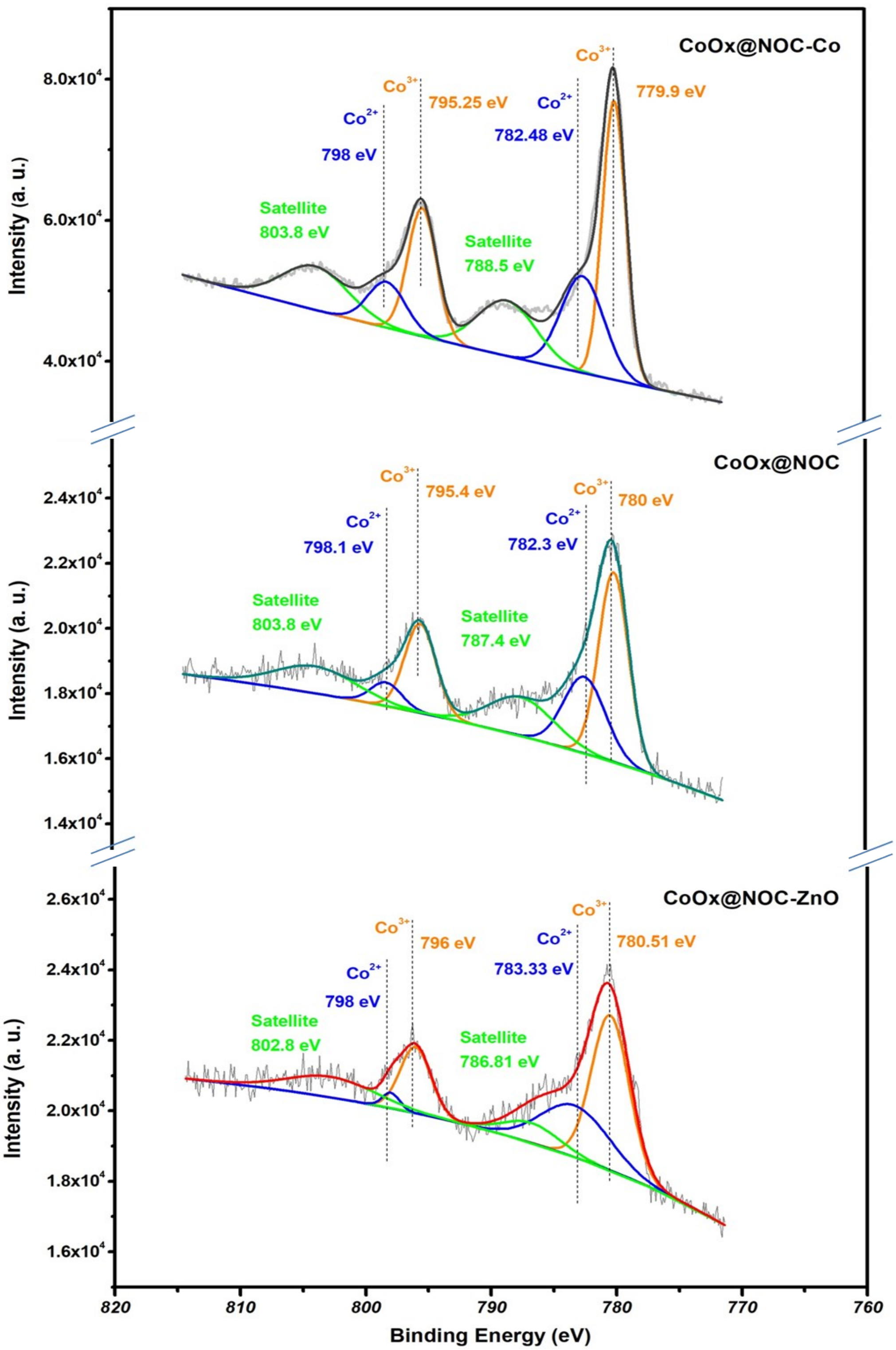


*Figure S7: The deconvolution of Co2p XPS high resolution spectra*

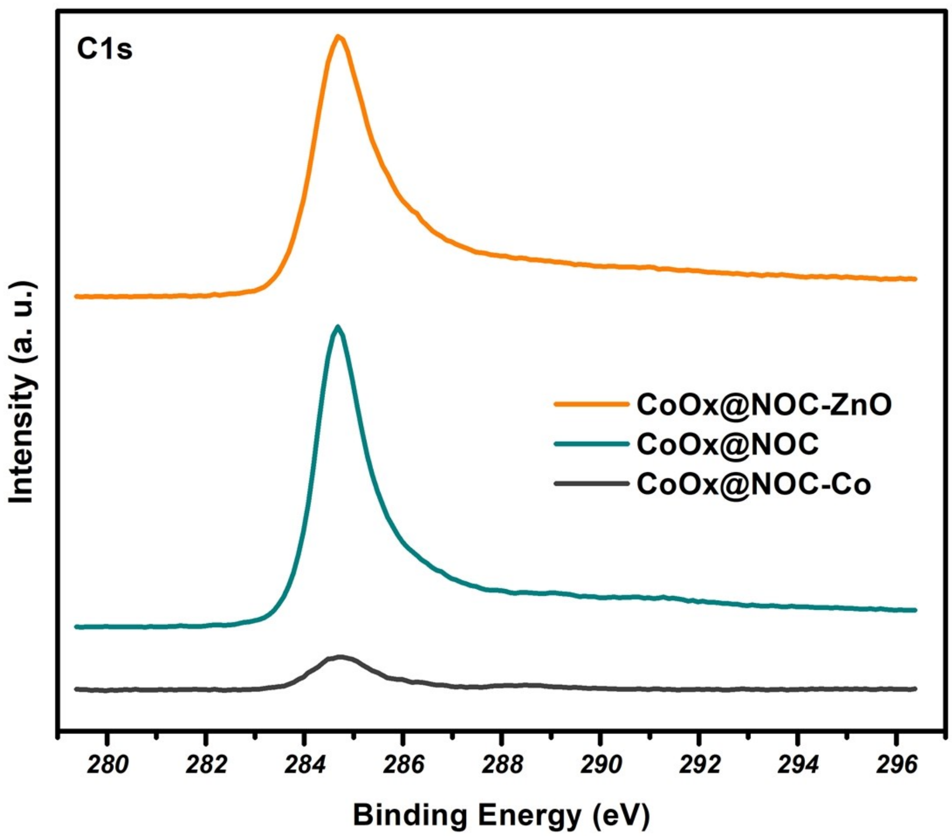


***Figure S8: C1s XPS high resolution spectrums***

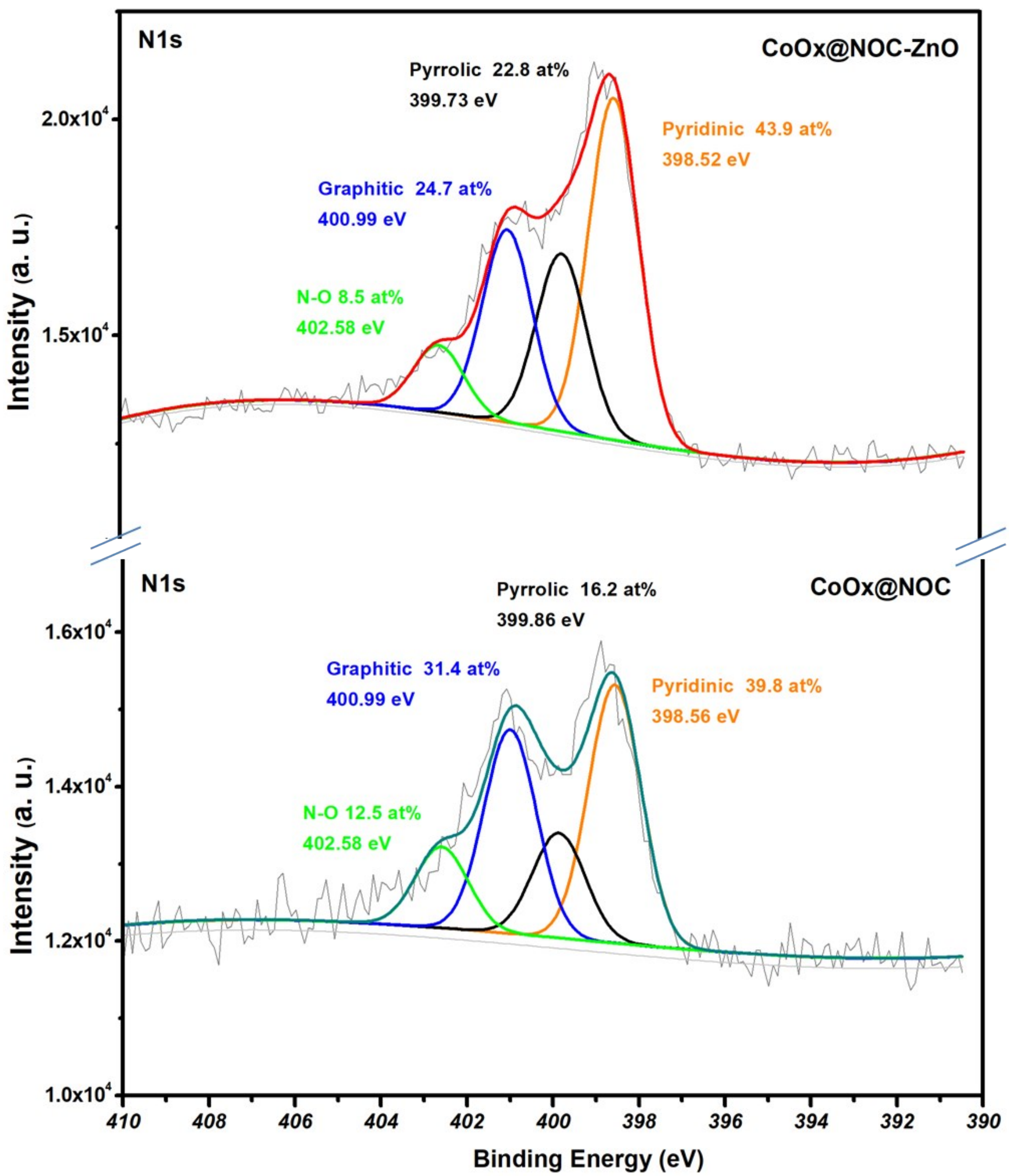


***Figure S9: The deconvolution of N1s XPS high resolution spectrums of CoOx@NOC-ZnO and CoOx@NOC***

a)

| *Sample* | *BET surface area* |
|---|---|
| ZnONR@ZIF-67-Co | 81.5161 m²/g |
| CoOx@NOC-Co | 102.7661 m²/g |
| ZnONR@ZIF-67 | 1906.0076 m²/g |
| CoOx@NOC | 291.9708 m²/g |
| ZnONR@ZIF-67-ZnO | 912.6553 m²/g |
| CoOx@NOC-ZnO | 456.9852 m²/g |

b)

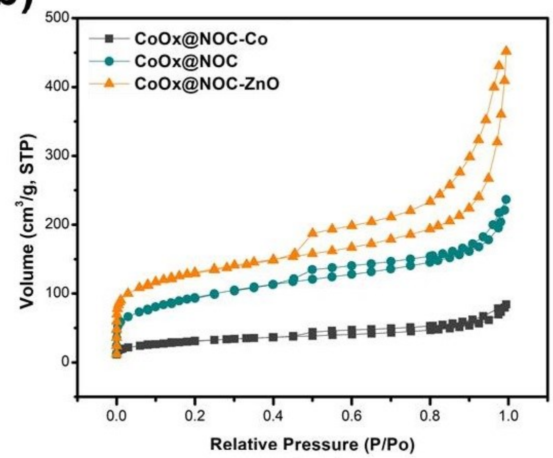


c)

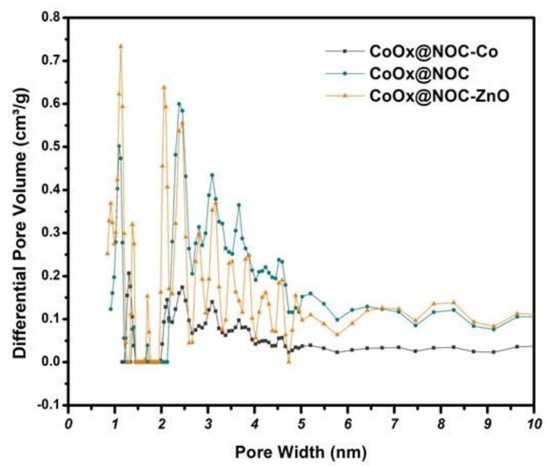


***Figure S10: Nitrogen adsorption and desorption analysis of the three samples. a) Table of BET surface areas of the three main ratios before and after pyrolysis; b) The $N_2$ adsorption isotherms of the three samples. c) The corresponding Pore-size distribution as derived from $N_2$ sorption.***

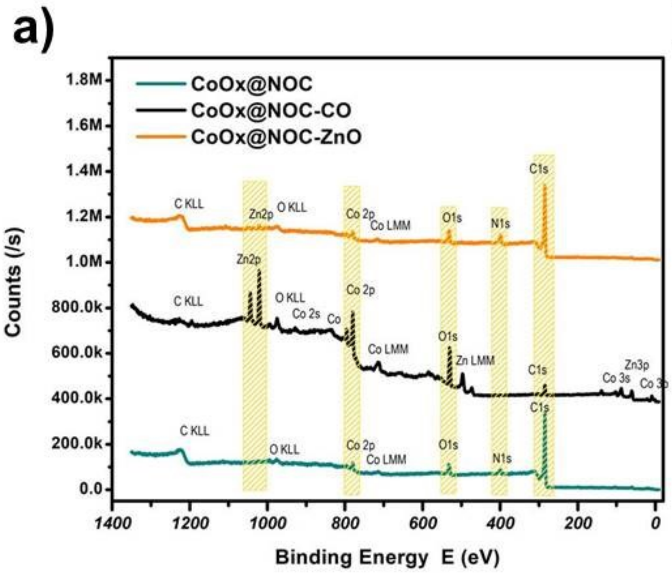


b)

| *Atomic percentage (%)* | CoOx@NOC | CoOx@NOC-ZnO | CoOx@NOC-Co |
|---|---|---|---|
| C1s | 85.99 | 81.12 | 25.4 |
| N1s | 5 | 9.09 | 0.42 |
| O1s | 7.12 | 7.64 | 45.21 |
| Co2p | 1.82 | 1.73 | 16.64 |
| Zn2p3 | 0.07 | 0.43 | 12.33 |

***Figure S11: a) XPS survey of the three samples; b) The elemental content percentages from XPS survey.***

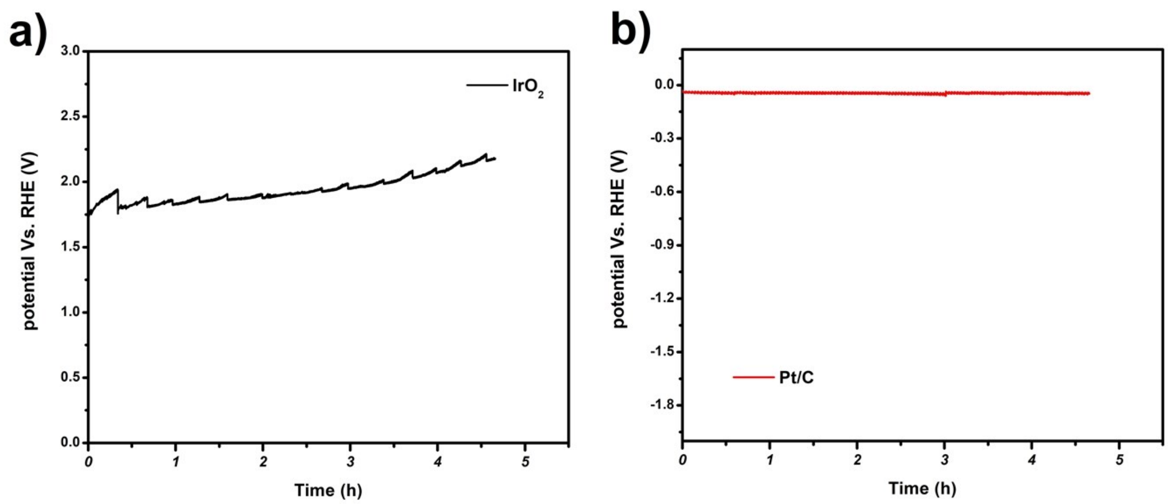


***Figure S12: I-t stability test of $IrO_2$ for OER at a current density of 15 mA $cm^{-2}$, and Pt/C for HER at 20 mA $cm^{-2}$.***

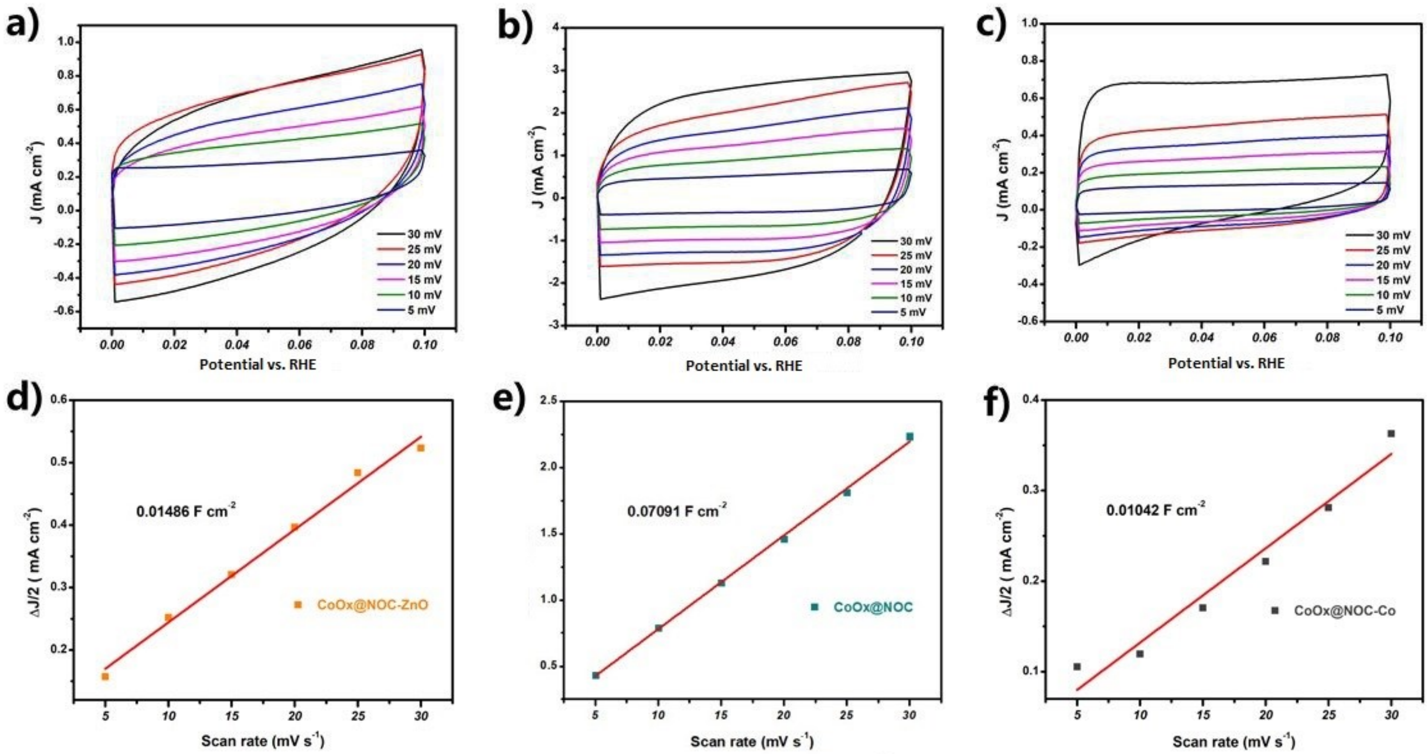


***Figure S13: CVs and correspondent Cdl curve of CoOx@NOC, CoOx@NOC-ZnO and CoOx@NOC-Co***

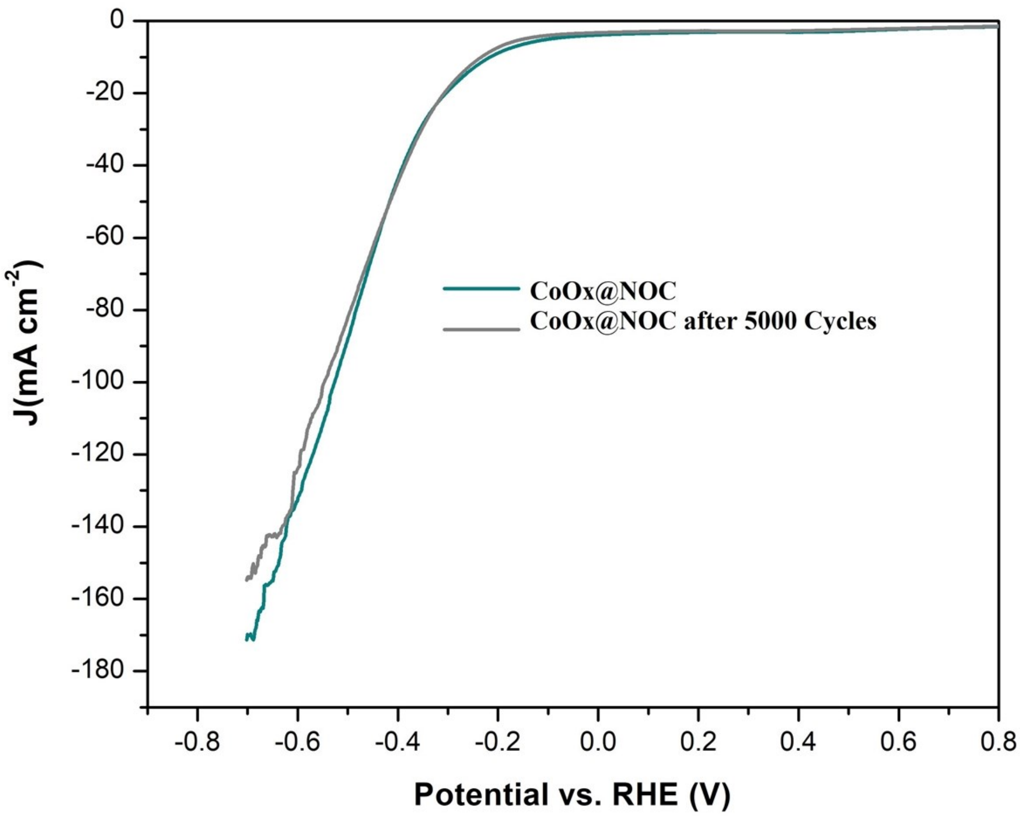


***Figure S14: HER LSV of CoOx@NOC after and before 5000 Cycles***

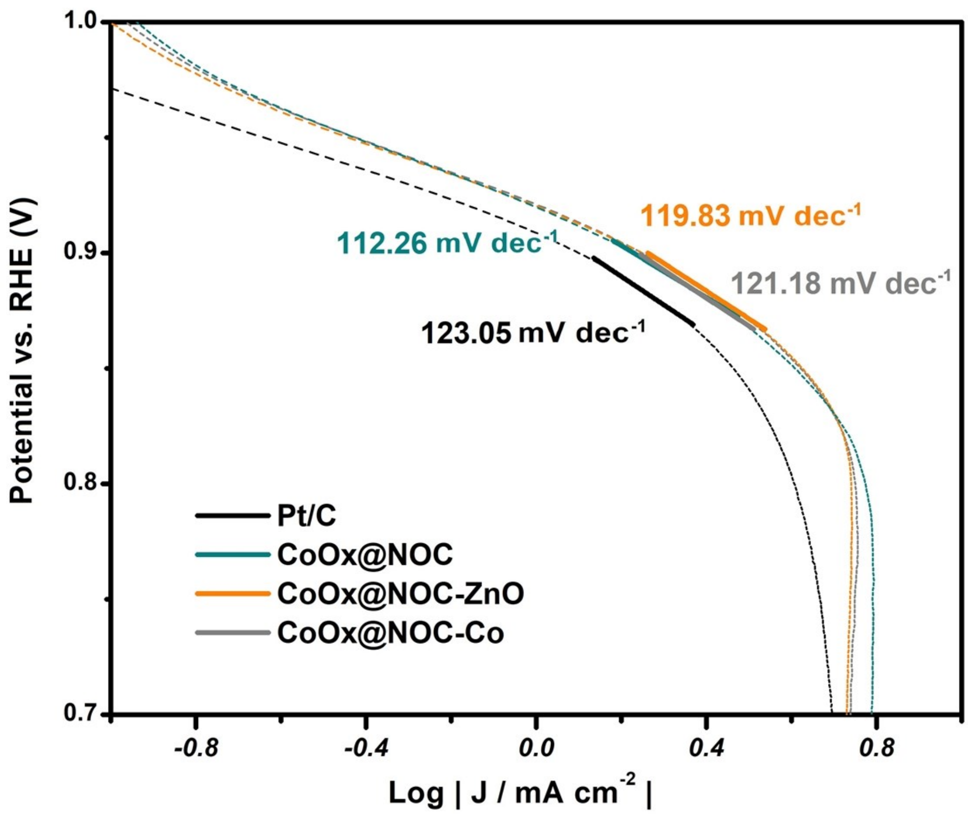


***Figure S15: ORR Tafel slopes of CoOx@NOC-Co***

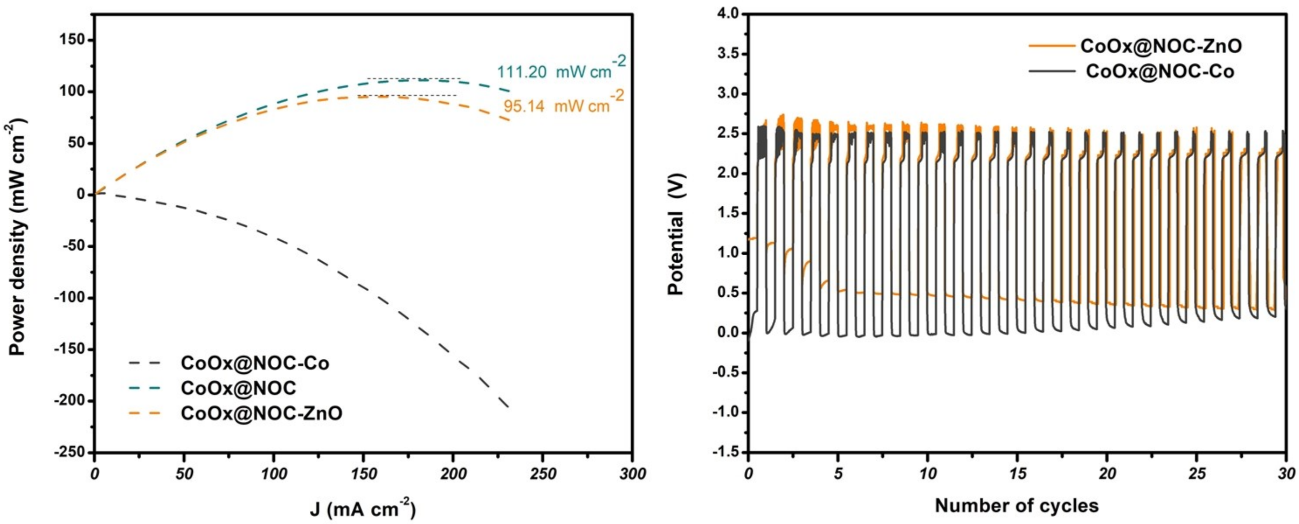


***Figure S16: Power densities of CoOx@NOC-ZnO and CoOx@NOC-Co along with CoOx@NOC based ZABs (a); Galvanostatic charge–discharge curves of CoOx@NOC-Co and CoOx@NOC-ZnO based ZABs.***

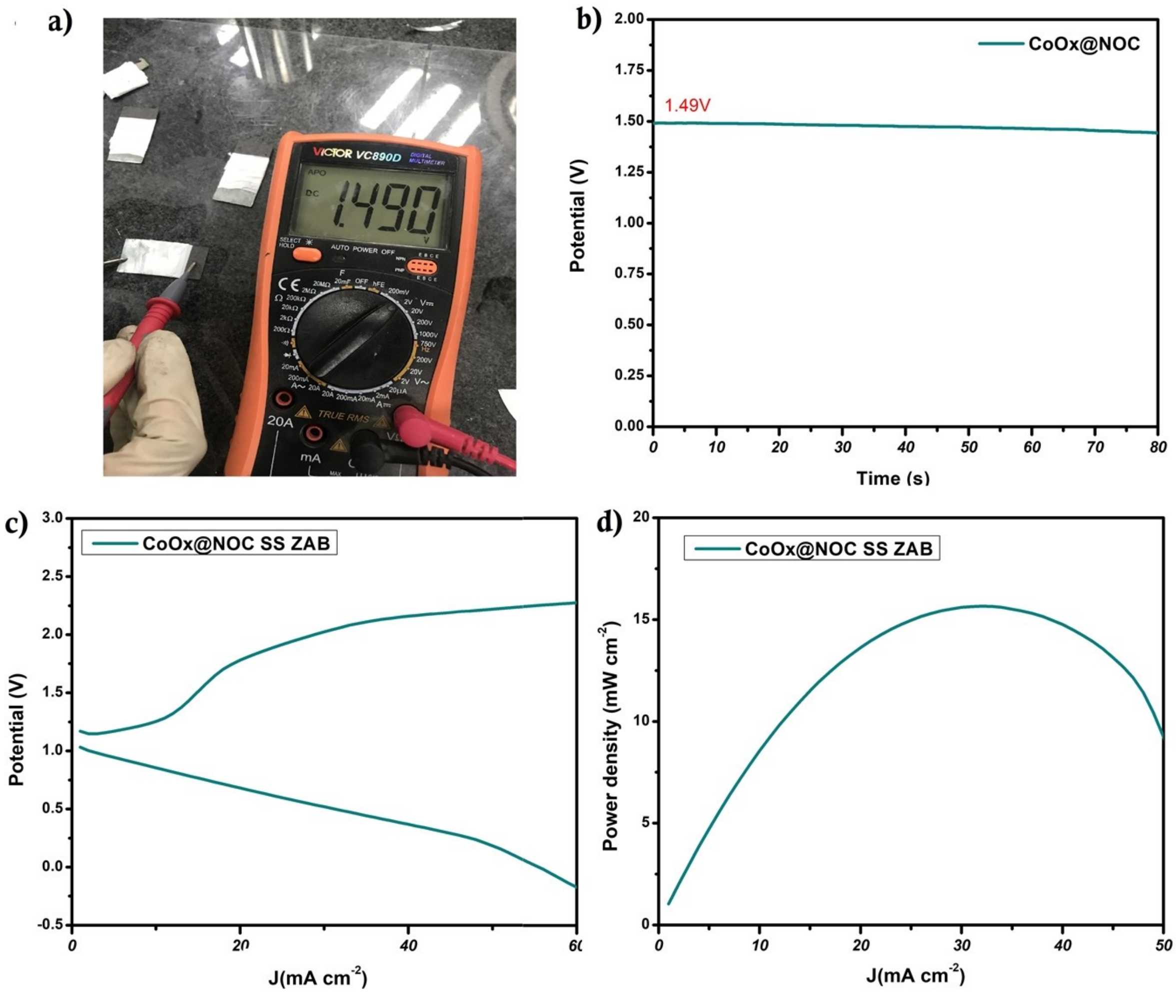


***Figure S17: Performance assessment of CoOx@NOC based SS ZAB, with 1 mg cm$^{-2}$ of mass loading on a surface of 4 cm². (a) Photograph of the SS ZAB and multimeter showing the open circuit potential; (b) Open circuit potential of CoOx@NOC based SS ZAB; (c) Charge–discharge polarization curves; (d) Power density curve.***

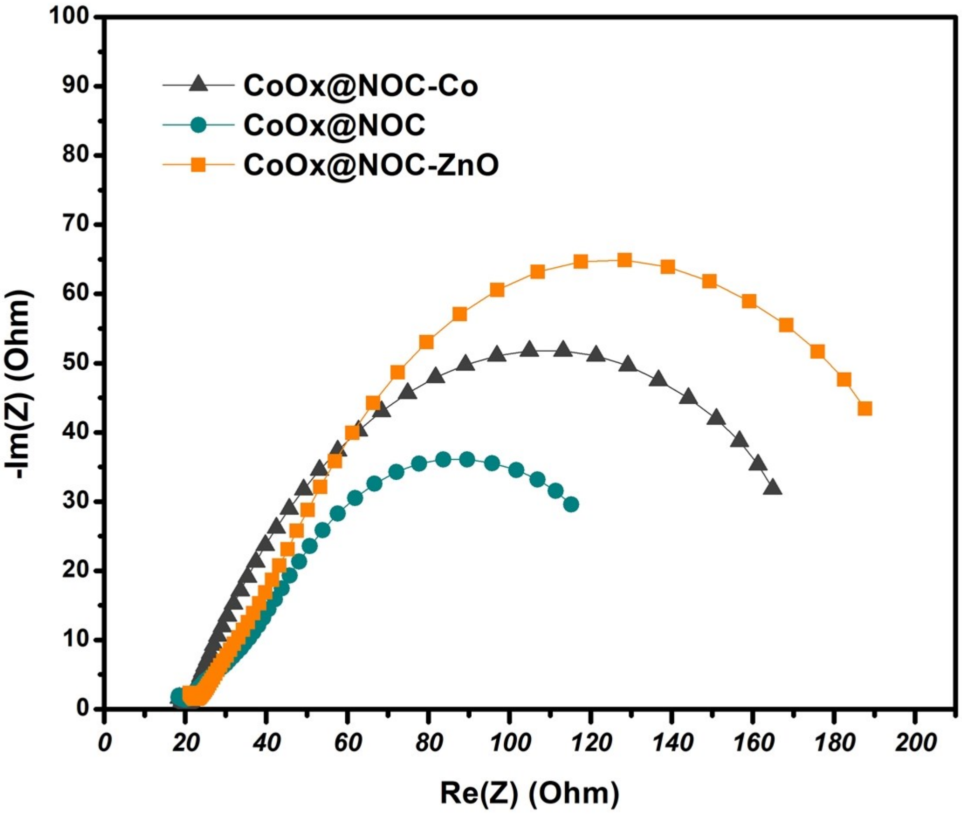


***Figure S18: Nyquist plots of CoOx@NOC-ZnO, CoOx@NOC, and CoOx@NOC-Co at 0.6 V in a frequency range of 100 kHz to 1 Hz, with an amplitude of 5 mV.***

***Table S3. Comparison of the electrocatalytic activity of Co-Carbon based bifunctional***

| Materials | OER $E_{j=10}$ (V) | ORR $E_{onset}$ (V) | $E_{1/2}$ (V) | Maximum current density (mA $cm^{-2}$) | ΔE | Loading | References |
|---|---|---|---|---|---|---|---|
| **CoOx@NOC** | 1.48 | 0.96 | 0.86 | -6.15 | 0.62 | 0.75 mg $cm^{-2}$ | Current work |
| **CoOx@NOC-ZnO** | 1.55 | 0.95 | 0.87 | -5.57 | 0.69 | 0.75 mg $cm^{-2}$ | Current work |
| **CoOx@NOC-Co** | 1.56 | 0.96 | 0.87 | -5.59 | 0.7 | 0.75 mg $cm^{-2}$ | Current work |
| **Pt/C** | - | 0.96 | 0.86 | -5.15 | - | 0.75 mg $cm^{-2}$ | Current work |
| **$IrO_2$** | 1.75 | - | - | - | - | 0.75 mg $cm^{-2}$ | Current work |
| **CoNC-CNF-1000** | 1.68 | - | 0.8 | | - | | [2] |
| **Co(OH)F/$CuCo_2S_4$** | 1.40 | | 0.8 | | | | [3] |
| **ZCP-CFs-900** | - | - | 0.805 | -5.6 | - | | [4] |
| **P-doped ZIF8-derived carbons** | - | - | 0.77 | -5.7 | - | | [5] |
| **$Fe_{0.3}Co_{0.7}$/NC cages** | - | - | 0.88 | -6 | - | | [6] |
| **NC@GC** | 1.57 | - | - | - | - | | [7] |
| **Co-N-CNT** | 1.69 | 0.97 | 0.9 | ~ -5.77 | 0.79 | | [8] |
| **N-GCNT/FeCo** | 1.59 | 0.97 | 0.87 | | 0.72 | | [9] |
| **$Co_3O_4$ /NPGC** | 1.68 | 0.97 | 0.84 | ~ -5.9 | 0.84 | | [10] |
| **NCNTFs** | 1.6 | 0.97 | 0.87 | ~ -5.2 | 0.73 | | [11] |
| **P,S-CNS** | 1.59 | 0.97 | 0.87 | - | 0.72 | | [12] |

| | | | | | | |
|---|---|---|---|---|---|---|
| **N-GRW** | 1.59 | 0.92 | 0.84 | - | 0.75 | [13] |
| **N, S-CN** | 1.64 | 0.91 | 0.76 | - | 0.88 | [14] |
| **Cu@NCNT/CoxOy** | 1.6 | 0.95 | 0.82 | ~ -5.6 | 0.78 | [15] |
| **NPMCs** | 1.58 | 0.94 | 0.85 | | 0.73 | [16] |

All values in the table above are vs. RHE.

***Table S4. Comparison of the BET surface area, $C_{dl}$, and active sites of trifunctional electrocatalysts:***

| Materials | Surface Area ($m^2\ g^{-1}$) | $C_{dl}$ ($mF\ cm^{-2}$) | Ref |
|---|---|---|---|
| **CoOx@NOC** | *292* | *70.9* | ***This Work*** |
| **CoOx@NOC-ZnO** | *457* | *14.8* | ***This Work*** |
| **CoOx@NOC-Co** | *103* | *10.25* | ***This Work*** |
| **Cu-Foam@CuCoNC500** | - | *64.85* | [17] |
| **CoSA + $Co_9S_8$/HCNT** | *636* | *51.33* | [18] |
| **GH-BGQD** | *320* | - | [19] |
| **CoSx@ $Cu_2MoS_4$- $MoS_2$/NSG** | *204* | *17* | [20] |
| **$Co_{5.47}N$@N-rGO-750** | *144* | *13.5* | [21] |
| **NiFe(II,III)-LDH** | - | *1.45* | [22] |
| **$Fe_{0.5}Ni_{0.5}$@N-GR** | *106* | *12* | [23] |

***Table S5. Comparison of the trifunctional electrocatalysts employed in Zn-air battery powered overall water splitting:***

| Materials | Zn-air battery | | | | Overall Water Splitting | Date | Ref |
|---|---|---|---|---|---|---|---|
| | Liquid-electrolyte battery | | | Solid-state battery | | | |
| | Open potential (V) | Specific capacity (mAh $g^{-1}_{zn}$) at 10 mA $cm^{-2}$ | Max. Power density (mW $cm^{-2}$) | Open potential (V) | Overpotential at 10 mA $cm^{-2}$ | | |
| CoOx@NOC | 1.57 | 757 | 141.65 | 1.49 | 1.51 | - | This Work |
| Cu-Foam@CuCoNC500 | 1.4 | 798 | 140 | 1.31 | 1.52 | 2019 | 17 |
| CoSA + $Co_9S_8$/HCNT | 1.45 | 788 (at 100 mA $cm^{-2}$) | 177.33 | 1.41 | 1.59 | 2020 | 18 |
| FeCo/$Co_2P$@NPCF | 1.44 | - | 154 | 1.257 | 1.68 | 2020 | 24 |
| GH-BGQD | 1.40 | 687 | 112 | 1.40 | 1.61 | 2019 | 19 |
| CoSx@ $Cu_2MoS_4$-$MoS_2$/NSG | 1.44 | - | (Solid-State) 40 | 1.442 | 1.60 | 2020 | 20 |
| $Co_{5.47}N$@N-rGO-750 | 1.45 | 788.5 | 121 | 1.4 | - | 2019 | 21 |
| NOGB-800 | 1.5 | - | 111.9 | - | 1.65 | 2019 | 22 |
| NiCoOS | - | - | 90 | - | 1.52 | 2019 | 25 |
| NiFe(II,III)-LDH | 1.26 | - | - | - | 1.54 | 2019 | 26 |
| $Fe_{0.5}Ni_{0.5}$@N-GR | 1.482 | 765 | 85 | 1.352 | 1.69 | 2018 | 23 |

***Supporting references***


1 K. Zhou, B. Mousavia, Z. Luo, S. Phatanasri, S. Chaemchuen, *Journal of Materials Chemistry A*, 2017, **5**, 952.
2 W. Zhang, X. Yao, S. Zhou, X. Li, L. Li, Z. Yu and L. Gu, *Small*, 2018, **14**, 1800423.
3 X. Ding, Y. Xia, Q. Li, S. Dong, X. Jiao and D. Chen, *ACS Applied Materials & Interfaces*, 2019, **11**, 7936–7945.
4 C. Liu, J. Wang, J. Li, J. Liu, C. Wang, X. Sun, J. Shen, W. Han and L. Wang, *Journal of Materials Chemistry A*, 2017, **5**, 1211–1220.
5 W. Zhang, Z. Y. Wu, H. L. Jiang and S. H. Yu, *Journal of the American Chemical Society*, 2014, **136**, 14385–14388.
6 B. Y. Guan, Y. Lu, Y. Wang, M. Wu and X. W. D. Lou, *Advanced Functional Materials*, 2018, **28**, 1–10.
7 X. Wang, T. Gao, F. Han, Z. Ma, Z. Zhang, J. Li and C. Wang, *Nano Energy*, 2016, **16**, 30465.
8 T. Wang, Z. Kou, S. Mu, J. Liu, D. He, I. S. Amiinu, W. Meng, K. Zhou, Z. Luo, S. Chaemchuen and F. Verpoort, *Advanced Functional Materials*, 2018, **28**, 1705048.
9 K. Sakaushi, A. Lyalin, S. Tominaka, T. Taketsugu and K. Uosaki, *ACS Nano*, 2017, **11**, 1770−1779.
10 G. Li, X. Wang, J. Fu, J. Li, M. G. Park, Y. Zhang, G. Lui and Z. Chen, *Angewandte Chemie - International Edition*, 2016, **55**, 4977–4982.
11 B. Y. Xia, Y. Yan, N. Li, H. Bin Wu, X. W. D. Lou and X. Wang, *Nature Energy*, 2016, **1**, 1–8.
12 S. S. Shinde, C. H. Lee, A. Sami, D. H. Kim, S. U. Lee and J. H. Lee, *ACS Nano*, 2017, **11**, 347–357.
13 H. B. Yang, J. Miao, S.-F. Hung, J. Chen, H. B. Tao, X. Wang, L. Zhang, R. Chen, J. Gao, H. M. Chen, L. Dai and B. Liu, *Science Advances*, 2016, **2**, e1501122–e1501122.
14 Q. Tang, Y. Cui, J. Wu, D. Qu, A. P. Baker, Y. Ma, X. Song and Y. Liu, *Nano Energy*, 2017, **41**, 377–386.
15 X. Zhao, F. Li, R. Wang, J. M. Seo, H. J. Choi, S. M. Jung, J. Mahmood, I. Y. Jeon and J. B. Baek, *Advanced Functional Materials*, 2017, **27**, 1605717.
16 J. Zhang, Z. Zhao, Z. Xia and L. Dai, *Nature Nanotechnology*, 2015, **10**, 444–452.
17 H. Sun, Q. Li, Y. Lian, C. Zhang, P. Qi and Q. Mu, *Applied Catalysis B: Environmental*, 2019, **263**, 118139.
18 Y. Li, R. Cao, L. Li, X. Tang, T. Chu, B. Huang, K. Yuan and Y. Chen, *Small*, 2020, **16**, 1906735.
19 T. Van Tam, S. G. Kang, M. H. Kim, S. G. Lee and S. H. Hur, *Advanced Energy Materials*, 2019, **9**, 1900945.
20 D. C. Nguyen, D. T. Tran, T. Luu, L. Doan, D. H. Kim, N. H. Kim and J. H. Lee, *Advanced Energy Materials*, 2020, **10**, 1903289.
21 X. Shu, S. Chen, S. Chen, W. Pan and J. Zhang, *Carbon*, 2019, **157**, 234.
22 Q. Hu, G. Li, G. Li, X. Liu, B. Zhu, X. Chai and Q. Zhang, *Advanced Energy Materials*, 2019, **9**, 1803867.
23 P. Liu, D. Gao, W. Xiao, L. Ma, K. Sun, P. Xi, D. Xue and J. Wang, *Advanced Functional*

*Materials*, 2018, **28**, 1706928.
24 Q. Shi, Q. Liu, Y. Ma, Z. Fang, Z. Liang, G. Shao, B. Tang and W. Yang, *Advanced Energy Materials*, 2020, **10**, 1903854.
25 Z. Bai, S. Li, J. Fu, Q. Zhang, F. Chang, L. Yang, J. Lu and Z. Chen, *Nano Energy*, 2019, **58**, 680–686.
26 X. Meng, J. Han, L. Lu, G. Qiu, Z. L. Wang and C. Sun, *Small*, 2019, **15**, 1902551.